

A boundary integral based particle initialization algorithm for Smooth Particle Hydrodynamics

Parikshit Boregowda*, Gui-Rong Liu

College of Engineering and Applied Science, University of Cincinnati, Cincinnati, Ohio, USA

Abstract

Algorithms for initializing particle distribution in SPH simulations of complex geometries have been proven essential for improving the accuracy of SPH simulations. However, no such algorithms exist for boundary integral SPH models, which can model complex geometries without needing virtual particle layers. This study introduces a Boundary Integral based Particle Initialization (BIPI) algorithm. It consists of a particle-shifting technique carefully designed to redistribute particles to fit the boundary by using the boundary integral formulation for particles adjacent to the boundary. The proposed BIPI algorithm gives special consideration to particles adjacent to the boundary to prevent artificial volume compression. It can automatically produce a "uniform" particle distribution with reduced and stabilized concentration gradient for domains with complex geometrical shapes. Finally, a number of examples are presented to demonstrate the effectiveness of the proposed algorithm.

Keywords: Boundary integral SPH, Particle Packing, Particle Shifting Technique, SPH initialization

1 Introduction

Smooth Particle Hydrodynamics (SPH) is a mesh-free numerical method that relies on a kernel function, also called a smoothing kernel, W , to approximate field variables[1]. The construction of an appropriate smoothing kernel theoretically allows the determination of higher-order derivatives of a field variable[2]. Nevertheless, practical implementations of the smoothing kernel focus on approximating the field and its derivatives using the kernel (W) and its first derivative (∂W).

The construction of the smoothing kernel allows for kernel-consistent conditions, which include $\int W = 1$ and $\int \partial W = 0$. However, in practical computational simulations utilizing summations for finite SPH particles, represented as $\sum W$ and $\sum \partial W$, deviations from the kernel consistent conditions arise, introducing errors into particle approximations. While efforts to enhance SPH accuracy using normalization techniques exist, they inadvertently compromise the conservative nature of the SPH formulation[3,4].

Conservative SPH formulations, crucial for momentum and energy conservation, strictly adhere to kernel consistency[5]. The uniform distribution of particles notably influences their accuracy. Thus, methodologies in the literature that improve particle distribution uniformity, such as particle packing for initialization[6–8], particle shifting for flow evolution[9–11], and ALE SPH formulations, directly impact simulation quality[12].

Another significant challenge in SPH emerges near domain boundaries when a smoothing kernel is truncated. Traditionally, addressing this issue involves adding layers of virtual particles[13,14], a progressively complex approach with intricate boundary shapes. Alternatively, considering the boundary integral terms of SPH formulations has gained attention[15–18], offering a promising avenue to overcome the limitations of virtual particles.

In an effort to achieve a uniform particle distribution before commencing a simulation, Monaghan[19] introduced a method involving a high damping term to initiate simulations, allowing particles to settle into equilibrium positions. However, this approach significantly increases computational demands and has been observed to lead to particle resettlement at the onset of the actual numerical simulation. Subsequently, Colagrossi et al. [6] introduced an effective particle packing scheme, emphasizing the importance of preventing particle resettlement under static conditions. Considerations for particle resettlement have also been explored by Litvinov et al.[20], demonstrating enhanced convergence characteristics of Smoothed Particle Hydrodynamics (SPH) formulations for uniform particle distribution. More recently, Negi et al. [7] presented an improved particle packing algorithm tailored for complex shapes by integrating the approaches of [6] and [21]. However, the methodologies of [6,7,19,22] use the virtual particles to model boundaries, making them incompatible with the boundary integral SPH model.

Moreover, our attempts to modify existing packing algorithms, incorporating damping terms to achieve stability near the boundary with a purely boundary integral model, have proven challenging. While the algorithm of Jiang et al [21] can pack particles without having to define ghost particles, their algorithm is designed specifically for blue noise sampling. Additionally, modifying their algorithm would still lead to particles on the boundary – however, in SPH simulations, we require the particles to be strictly inside the boundary. A more promising algorithm to initialize particle distribution without dealing with virtual or ghost particle layers for boundary models is the CAD BPG algorithm and its variants [23,24]. However, in addition to requiring level

set information, their algorithm uses traditional SPH formulation, which does not address the inaccuracies of the truncated kernel. Thus, a compelling need exists to develop a dedicated packing algorithm for boundary integral SPH models by directly employing the boundary integral formulations.

2 Boundary modeling in SPH

2.1 The basic boundary integral formulation

Boundary integral formulations of Smooth Particle Hydrodynamics allow for handling boundaries by simply accounting for the otherwise neglected boundary integral in SPH derivative formulation,

$$\langle \partial_i f(\mathbf{x}) \rangle = - \int_{\partial(\Omega \cap \Omega_w)} f(\mathbf{x}') W(\mathbf{x} - \mathbf{x}', h) \hat{\mathbf{n}}_i dS' - \int_{\Omega \cap \Omega_w} f(\mathbf{x}') \partial_i W(\mathbf{x} - \mathbf{x}', h) dV' \quad (1)$$

As demonstrated in our previous work [25], a consistent analysis of the integral formulation (1) reveals that the necessary smoothing kernel properties are still violated at the boundary due to the truncated kernel (see Figure 1). For kernel consistency, the gradient of the field is modified as,

$$\langle \nabla f_a \rangle_{KC} = \frac{1}{\gamma_a} \left(\sum_b f_b \nabla_a W_{ab} \frac{m_b}{\rho_b} - \sum_s \int_{\partial(\Omega \cap \Omega_w)_s} f(\mathbf{x}'_s) W_{as'} \hat{\mathbf{n}}_s dS' \right) \quad (2)$$

Where, $\gamma_a = \int_{\Omega \cap \Omega_w} W(\mathbf{x} - \mathbf{x}', h) dV'$.

The boundary integral in (2) can be calculated in various ways. Here, we simply approximate the boundary integral as:

$$\int_{\partial(\Omega \cap \Omega_w)_s} f(\mathbf{x}'_s) W_{as'} \hat{\mathbf{n}}_s dS' = f_s \int_{\partial(\Omega \cap \Omega_w)_s} W_{as'} \hat{\mathbf{n}}_s dS' = f_s \nabla \gamma_{as} \quad (3)$$

Finally, γ_a and $\nabla \gamma_{as}$ is determined analytically for a smoothing kernel. The analytical calculations discussed in Leroy et al and Fieldman et al for the 2D Quintic Wendland kernel is adopted in the work here. Additionally, to effectively use boundary integral formulations for modelling complex shapes, we employ the no boundary particles (NBP) approach, where the domain boundary is directly represented by line segments (in 2D) and triangles (in 3D). The size of the boundary segment itself will depend on the numerical integration technique used for the first term in (3).

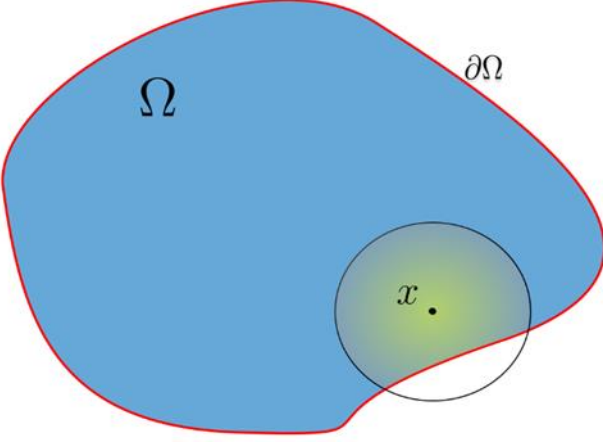


Figure 1 The smoothing domain Ω_w is truncated by the boundary of the domain Ω

2.2 Measuring uniform distribution

Achieving a uniform particle distribution plays a crucial role in minimizing the error associated with calculating SPH approximations, as it brings the terms $\sum_b V_b W_{ab}$ and $\sum_b \nabla_a W_{ab} V_b$ closer to 1 and 0, for uniform distribution. This also implies that the uniformity of particle distribution for some complex geometry is dependent solely on the smoothing kernel and the smoothing length used.

Now, if we employ the boundary integral model of SPH, a constant field, and its gradient is given by,

$$\langle C_a \rangle = \frac{\sum_b V_b W_{ab}}{\gamma_a} \quad (4)$$

and,

$$\langle \nabla C_a \rangle = \frac{1}{\gamma_a} \left(\sum_b \nabla_a W_{ab} V_b - \sum_s \nabla \gamma_{as} \right) \quad (5)$$

Now to define uniform particle distribution, we would require,

$$\langle C_a \rangle \rightarrow 1 \quad (6)$$

$$\langle \nabla C_a \rangle \rightarrow \mathbf{0} \quad (7)$$

The magnitude of error in achieving these limiting values, (6) and (7), is higher for truncated kernels compared to untruncated kernels, as discussed in [25]. It is important to note that achieving exact equality for (6) and (7) is not feasible due to the discretized nature of particle distribution and the integral approximation inherent in SPH kernels. However, the primary objective is to reduce the error in approaching these values while using the conservative form of SPH equations in practical simulations.

3 A Boundary Integral based Particle Initialization (BIPI) algorithm

3.1 Generating particles from computational geometry file: Step 1

The initial step in any particle initialization algorithm involves generating particles from the geometry file. This process can be executed in two ways: by substituting the underlying Cartesian grid (voxel in 3D and pixel in 2D) of the geometry's interior with particles or by meshing the geometry's volume and subsequently replacing each volume element with a particle. The former approach is commonly employed within the SPH community [26,27].

In our approach, we leverage the geometry's boundary information to generate particles relative to an underlying Cartesian grid, and we directly utilize the boundary elements for calculating the boundary integral in equation (3). This data is readily available in the STL file format for 3D geometries with triangles, while for 2D geometries, line elements are utilized to represent the boundary.

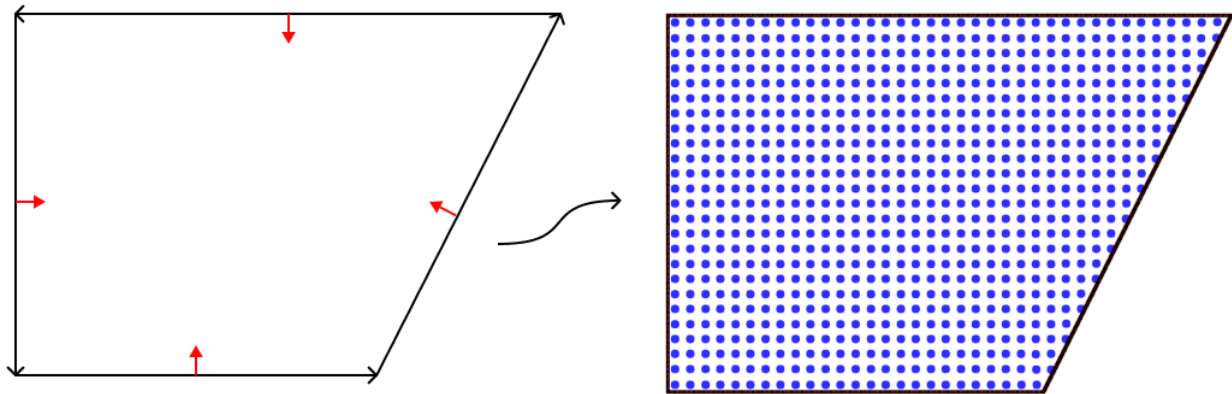


Figure 2 A point in polygon algorithm is used to generate one particle per cartesian cell using boundary edges and boundary sense to differentiate interior from exterior of polygon.

3.2 Shift particles using the concentration gradient: Step 2

The next step in the BIPI algorithm is to pack particles along the boundary while also aiming to achieve a uniform distribution. To achieve this, we start with the SPH pressure gradient formulation for particles in a symmetric form by simply adding $0 = f(\mathbf{x}) \int_{\partial(\Omega \cap \Omega_w)} W(\mathbf{x} - \mathbf{x}', h) \hat{n}_i dS' - \int_{\Omega \cap \Omega_w} \partial_i W(\mathbf{x} - \mathbf{x}', h) dV'$ to (1) and then converting it into its particle counterpart as,

$$\langle \nabla p_a \rangle = \frac{1}{\gamma_a} \left(\sum_b (p_a + p_b) \nabla_a W V_b - \sum_s (p_a + p_s) \nabla \gamma_{as} \right) \quad (8)$$

Assuming all particles have the same density and pressure, with pressure at the boundary equal to that inside, we aim for particles to reach equilibrium, which simplifies (8) to,

$$\ddot{\mathbf{x}}_a = -\frac{2 p_0}{\gamma_a \rho_0} \left(\sum_b \nabla_a W V_b - \sum_s \nabla \gamma_{as} \right) = -\frac{2 p_0}{\rho_0} \nabla C_a \quad (9)$$

A stable configuration is achieved when the acceleration in equation (9) is zero, necessitating ∇C_a to approach zero. In other words, equation (9) dictates particle movement to minimize the concentration gradient, akin to a Particle Shifting Technique (PST) as follows,

$$\delta \tilde{\mathbf{x}}_a = -D_a \nabla C_a \quad (10)$$

Where,

$$D_a = (\delta t)^2 \frac{2 p_0}{\rho_0} \quad (11)$$

The PST described in (10) closely resembles the one proposed by Lind et al. [10], based on Fick's law analogy. It has been widely utilized in recent years within SPH for its effectiveness in preventing tensile instability issues and improving simulation results. While PST models in SPH conventionally operate within the confines of virtual particle layers, the research conducted by [28] extended Lind's methodology for particle shifting to boundary integrals. However, applying the PST directly for particle initialization, particularly in proximity to the boundary, is not feasible.

To calculate the particle shift $\delta \mathbf{x}_a$ in the BIPI algorithm, we employ the following approach: Since equations (10) and (11) reduce to the diffusion law for PST, as discussed by Lind, we set $D_a = 0.5 h^2$. This value is derived from thermodynamic considerations of p_0 to be proportional to ρ_0 , and by imposing a CFL constraint on the time step δt . Specifically, $\delta t \leq C_{min} \left(\frac{h}{c_0} \right) \Rightarrow (\delta t c_0)^2 \leq (C_{min} h)^2$. Commonly, C_{min} is less than 1, with values such as 0.4 [1,29]. Using $C_{min} = 0.5$ we get, $D_a = 2(\delta t c_0)^2 = 0.5 h^2$. Next, to prevent extensive shifting of particles, we establish an upper limit of $|\delta \mathbf{x}_a| = 0.25 dx_r$, where dx_r is the average particle spacing.

Thus, reducing our particle shift equation to,

$$\delta \mathbf{x}_a = \begin{cases} \widetilde{\delta \mathbf{x}}_a & |\widetilde{\delta \mathbf{x}}_a| < 0.25 dx_r, \\ -0.25 dx_r \frac{\nabla C_a}{\|\nabla C_a\|} & 0.25 dx_r < |\widetilde{\delta \mathbf{x}}_a| \end{cases} \quad (12)$$

While using (12) directly can redistribute particles to minimize ∇C_a , it can inadvertently result in particles being positioned too close to the boundary. However, it is imperative that the layer of particles adjacent to the boundary remains uncompressed. Assuming a particle's volume is uniformly distributed in the radial direction, with a particle radius of $\frac{dx_r}{2}$, maintaining a uniform particle distribution dictates that the particle near the boundary should be positioned $\frac{dx_r}{2}$ away from the boundary. This issue is typically addressed in physics-driven simulations through the application of external forces by the boundary. For example, in flow simulations, the boundary pressure term, p_s in (8), increases as particles approach the boundary. While various methods for updating p_s have been explored in recent literature for fluid flows, implementing such techniques directly for BIPI would necessitate solving the complete set of fluid equations, thereby undermining the purpose of particle initialization schemes.

The acceleration due to the pressure gradient in (8) can be expressed in terms of concentration gradient and varying boundary pressure as,

$$\ddot{\mathbf{x}}_a = -\frac{2p_a}{\rho_a} \left[\nabla C_a - \frac{1}{\gamma_a} \sum_s \frac{1}{2} \left(\frac{p_s}{p_a} - 1 \right) \nabla \gamma_{as} \right] \quad (13)$$

Accurately modeling p_s proves challenging and relies on the method used to model volume compression. For instance, if we employ small non-linear springs at the boundary to simulate particle compression and apply conservative force, as shown in Figure 2a, the pressure variation becomes non-linear (Figure 2b). However, our numerical experiments have shown that a simple ramp function suffices to ensure particles remain approximately a radius away from the boundary (see Figure 2c). We opt for $p_s = 2 p_a$ in equation (13), yielding:

$$\widehat{\delta \mathbf{x}}_a = -D_a \left[\nabla C_a - \frac{\nabla \gamma_a}{2 \gamma_a} \right] \quad (14)$$

Applying an upper bound to the total particle shift, as before, we derive:

$$\delta \mathbf{x}_a = \begin{cases} \widehat{\delta \mathbf{x}}_a & |\widehat{\delta \mathbf{x}}_a| < 0.25 dx_r, \\ -0.25 dx_r \frac{\nabla C_a - \frac{\nabla \gamma_a}{2 \gamma_a}}{\left\| \nabla C_a - \frac{\nabla \gamma_a}{2 \gamma_a} \right\|} & 0.25 dx_r < |\widehat{\delta \mathbf{x}}_a| \end{cases} \quad (15)$$

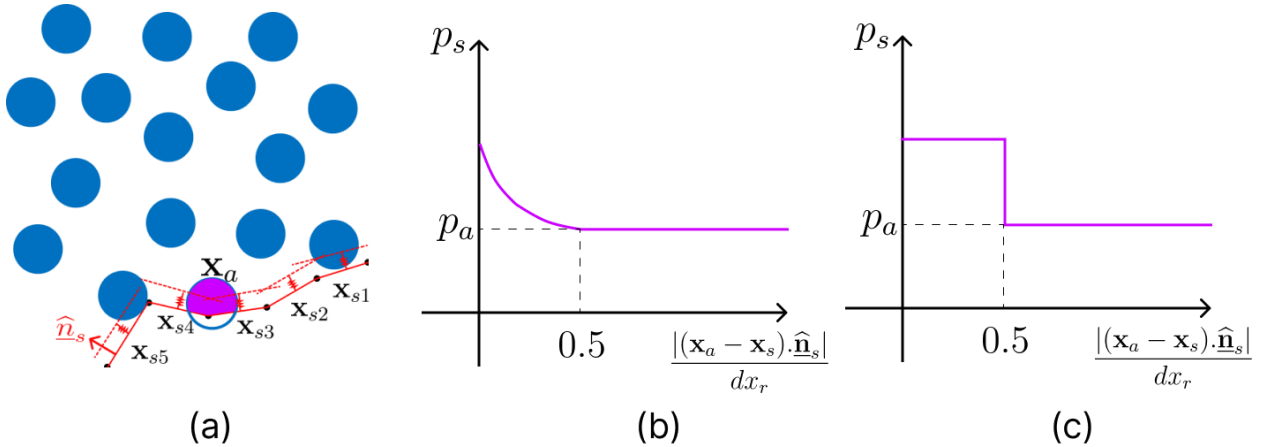


Figure 3 Modeling external repulsive force for particles immediately adjacent to the boundary. (a) Illustration of force exerted by particles on neighboring particles within their radius, (b) depiction of non-linear boundary pressure variation, and (c) representation of a ramp force acting on boundary particles.

Furthermore, we modify our algorithm to expedite settling time and minimize the computational overhead. This involves initially shifting particles with truncated kernels and subsequently shifting particles everywhere except those immediately adjacent to the boundary. This final adjustment applies when particles are generated on a background Cartesian grid. Otherwise, we recommend iteratively employing (15) in Step 2 until achieving the desired uniform configuration. As starting

on the Cartesian grid is generally the most practical approach, we outline our final modification as follows:

Step 2a: Employ (15) exclusively for particles adjacent to the boundary until the Total Particle Displacement (TPD) in this region converges. Untruncated particles located away from the boundary are not considered, significantly reducing computational load.

Step 2b: Freeze particles immediately adjacent to the boundary.

Step 2c: Continue particle shifting iterations using (15) for all particles, which essentially equates to using (12) since particles adjacent to the boundary are frozen in Step 2b. While waiting for particle displacement to converge, as in Step 2a, is possible, our numerous numerical experiments have determined that running Step 2c for just 1000 iterations is more than sufficient to minimize the concentration gradient to acceptable limits.

4 Results and Discussion

4.1 A simple Trapezoid geometry

To illustrate the BIPI algorithm discussed in the preceding section, we examine the trapezoidal geometry depicted in Figure 2. Initially, the geometry's interior is discretized into particles using the underlying Cartesian grid, establishing the starting configuration for Step 2. We closely examine the particle arrangement at the top-left and top-right corners of the trapezoidal geometry, as shown in Figure 4, to underscore the significance of employing a force-based equation (15), instead of equation (12).

It is evident that utilizing equation (12) for the BIPI algorithm causes particles to approach the boundary too closely, while others move away from it to counteract this proximity, illustrating that minimizing $|\nabla C_a|$ alone is insufficient to maintain a uniform configuration near the boundary. This observation is corroborated by the $|\nabla C_a|$ calculation for the starting configuration at the top-left corner, where, despite the particles following the boundary precisely, the $|\nabla C_a|$ value for truncated kernels remains non-zero. However, reducing $|\nabla C_a|$ for a given configuration enables reduced resettlement and noise when the physics-based simulation commences on the particle configuration. Additionally, employing equation (12) presents challenges in establishing a suitable stopping criterion for the BIPI algorithm. Monitoring configurations throughout the iteration cycles would then be necessary to identify an optimal configuration.

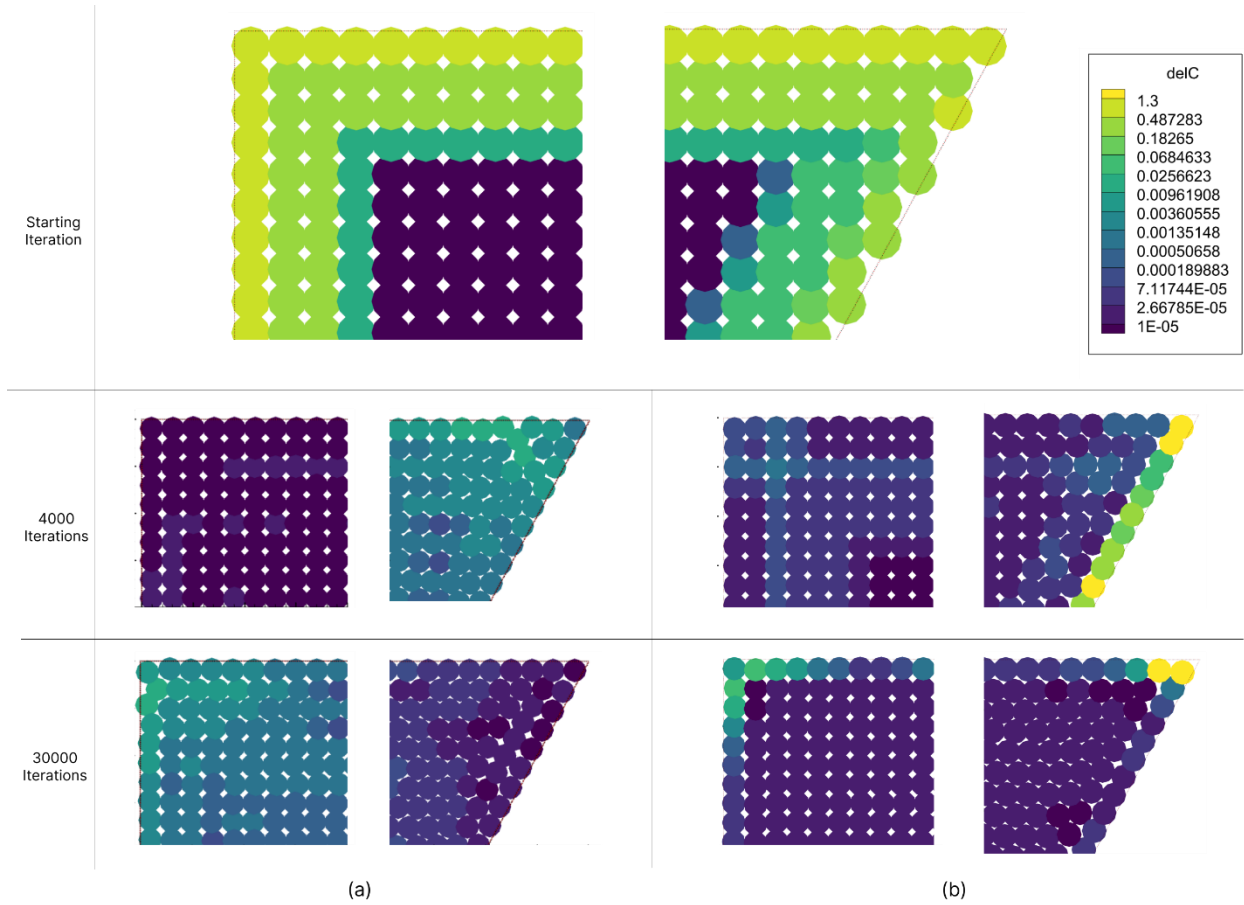


Figure 4 Comparison of BIPI for 30000 iterations using (a) Using equation (12), (b) using equation (13) with steps 2a, 2b, 2c.

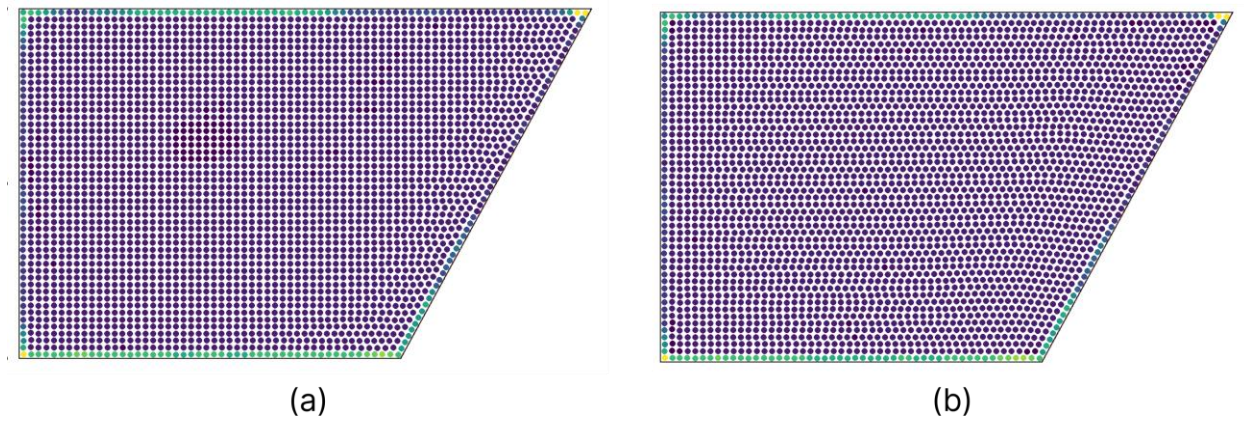


Figure 5 Scatter plot at (a) 7000 iterations, (b) 30000 iterations for the BIPI algorithm using equation (13) and following steps 2a, 2b, and 2c.

Conversely, employing equation (15) demonstrates that the BIPI algorithm facilitates effective particle resettlement along the boundary while simultaneously reducing $|\nabla C_a|$ overall. By

incorporating an external force in the formulation, the particles adjacent to the boundary maintain a consistent distance from it, approximately one radius away. Moreover, setting up the stopping criterion becomes more straightforward, utilizing the first plateau region of TPD to transition from Step 2a to Step 2b.

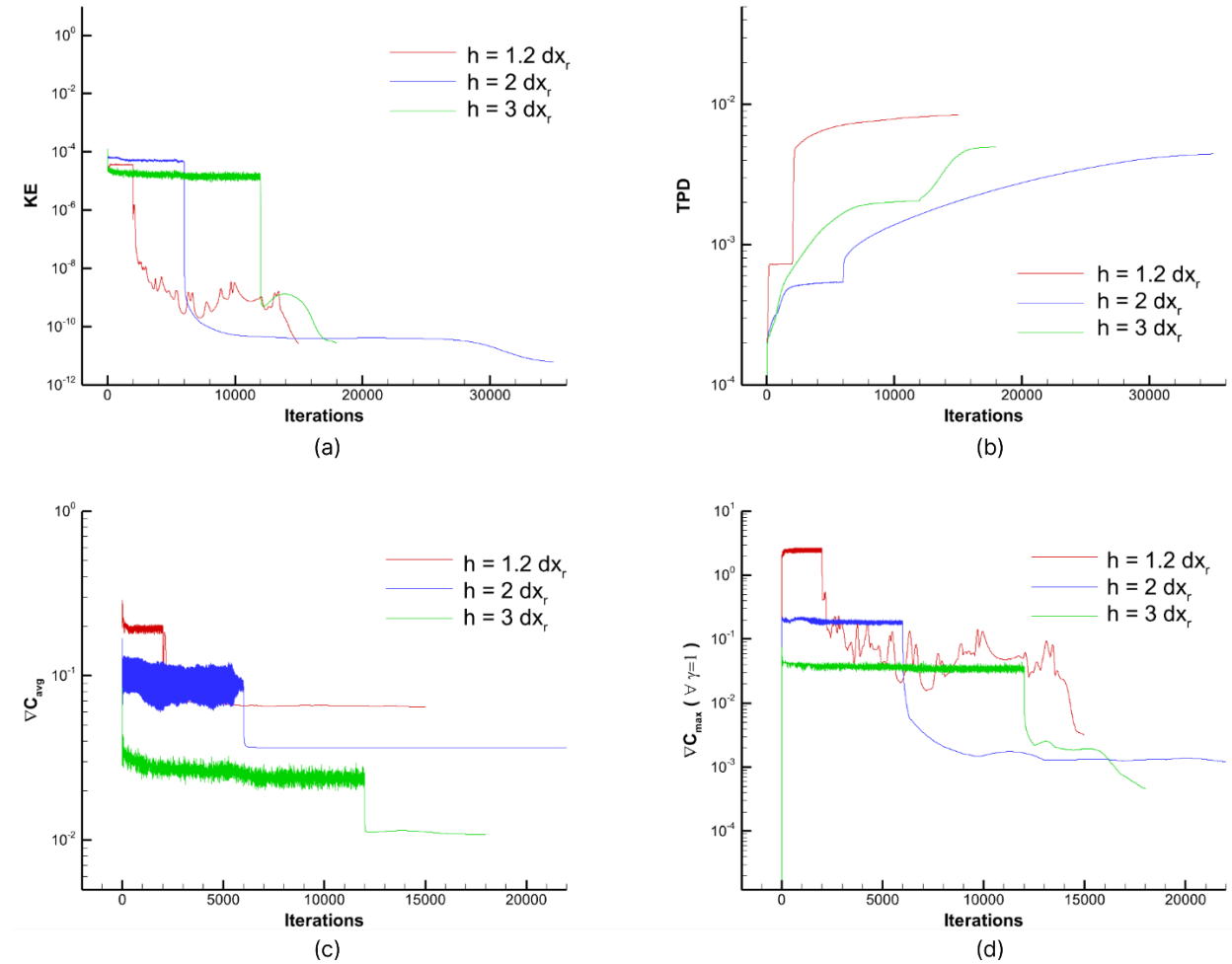


Figure 6 Evolution of (a) KE, (b) TPD, (c) $|\nabla C|_{avg}$, and (d) $|\nabla C|_{max}$ for particles with $\gamma = 1$, during the BIPI algorithm, for particle spacing $dx_r = 0.02m$ and varying smoothing length ratios.

Although continuing iterations in Step 3c until particles fully settle is feasible, our experience indicates minimal added benefit, as seen in the scatter plot of Figure 5. At a minimum, Step 3c should run a sufficient number of iterations to ensure that there is no abrupt change in concentration gradient between particles with $\gamma_a < 1$ and those with $\gamma_a = 1$. Our experience suggests that just 1000 steps suffice for $|\nabla C|_{avg}$ to decrease to a level beyond which additional resettlement does not lead to further reduction in $|\nabla C|_{avg}$. For the trapezoidal dam with $dx_r = 0.02m$ and $h =$

$2dx_r$, we observe TPD plateaus and Step 2a concludes after 6000 iterations. After an additional 1000 iterations, in Step 2c, we notice minimal changes in the values of various parameters in Figure 6.

We further evaluate the algorithm for different smoothing lengths, as shown in Figure 7. Although not depicted here, particle resettlement varies for different smoothing lengths, as the smoothing length influences the values of $|\nabla C_a|$ for each particle.

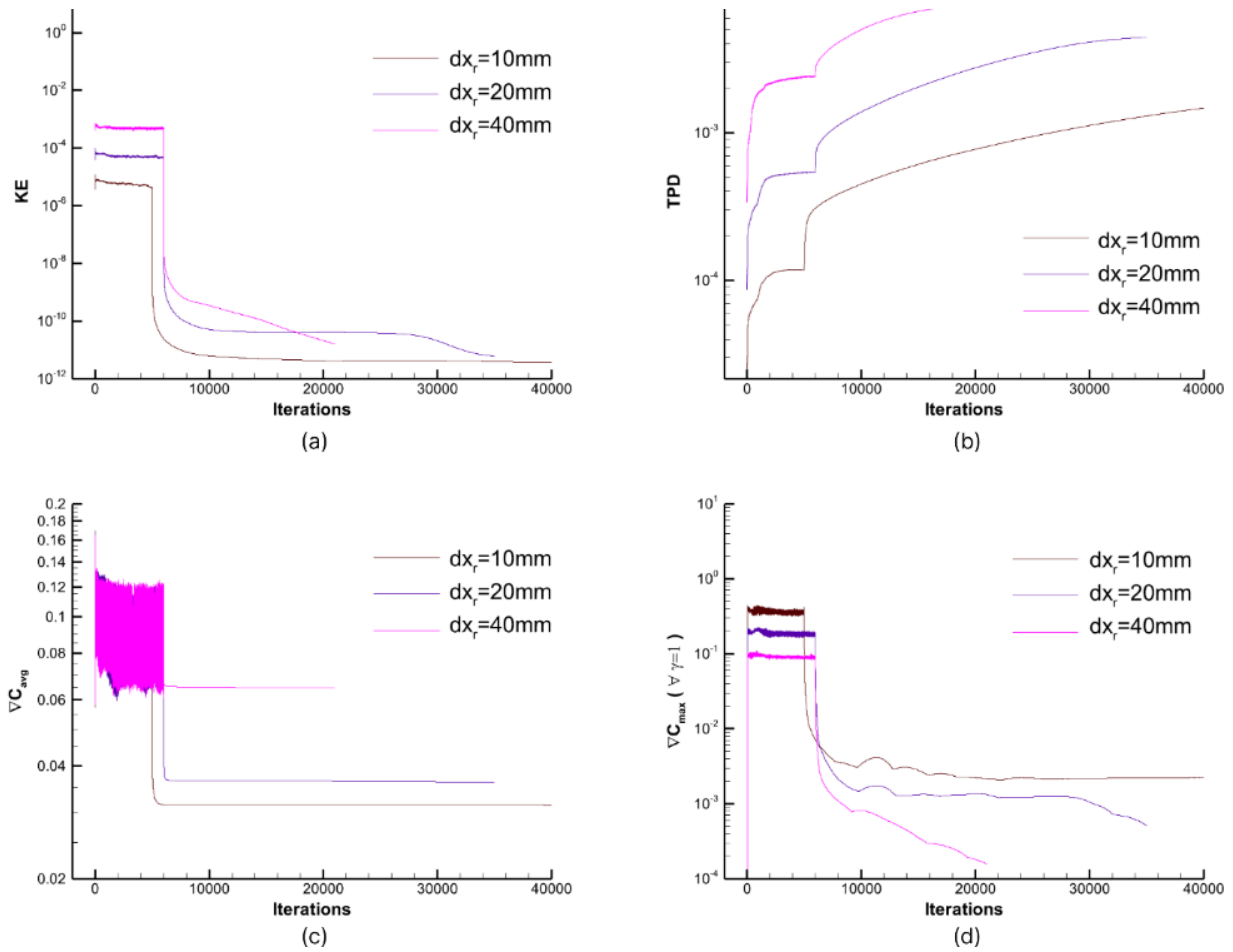


Figure 7 Evolution of (a) KE, (b) TPD, (c) $|\nabla C|_{avg}$, and (d) $|\nabla C|_{max}$ for particles with $\gamma = 1$, during the BIPI algorithm for various particle spacings.

4.2 Complex geometries

Finally, we showcase the algorithm's performance on two complex geometries: a 2D Bunny in Figure 8 and a NACA airfoil in Figure 9. We adhere to the BIPP algorithm in both cases, implementing steps 2a, 2b, and 2c.

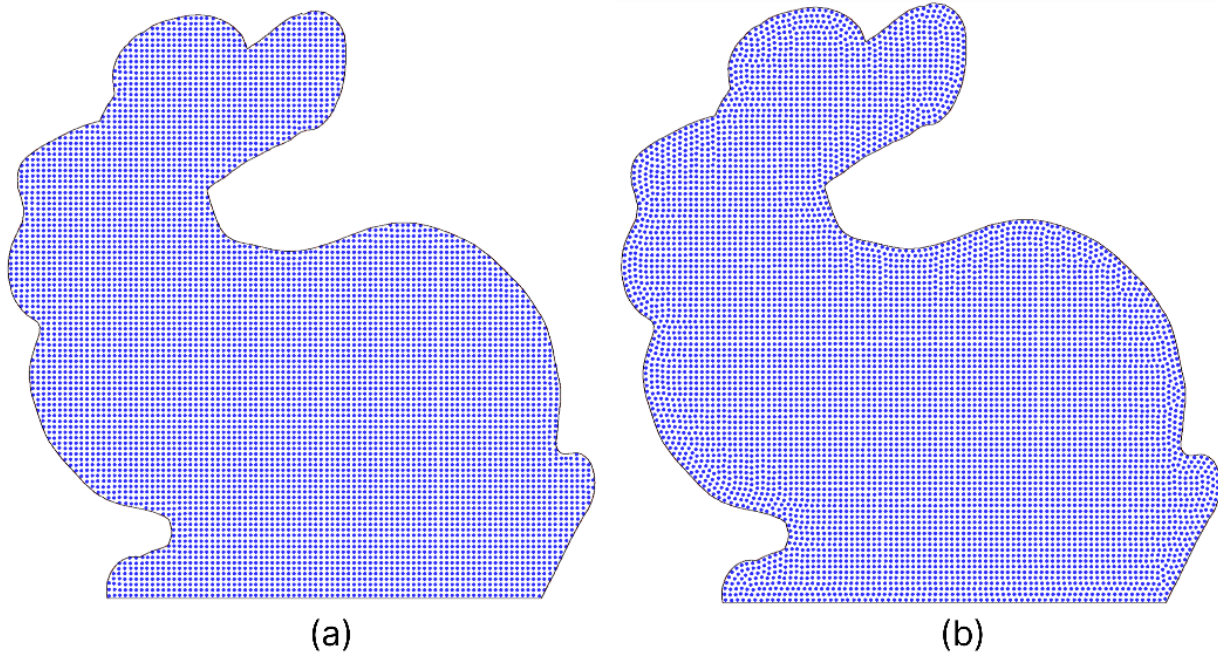


Figure 8 BIPP algorithm on Stanford 2D Bunny (a) Starting Configuration (b) Initialized particle distribution

For the 2D Bunny, Step 2a, which exclusively involves particles adjacent to the boundary with a truncated smoothing kernel, requires approximately 8000 steps. Subsequently, BIPP Step 2c is executed for an additional 1000 steps to achieve the configuration depicted in Figure 8b. In this configuration, particles near the boundary accurately follow its contours, resulting in an overall reduction in the concentration gradient. Further iterations of BIPP yield no significant changes in the overall concentration gradient and other parameters, as depicted in Figure 10.

Similar observations apply to the NACA airfoil case depicted in Figure 9. Here, we apply BIPP to both the fluid and airfoil structure, enabling us to attain a more uniform distribution relative to the boundary.

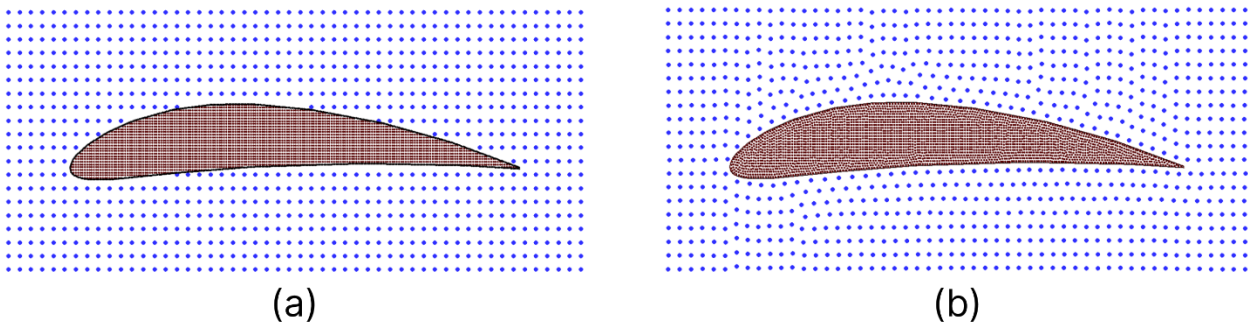


Figure 9 Application of the BIPP algorithm to a NACA6412 Airfoil with varying particle spacing for the airfoil structure and fluid domain. (a) Starting configuration and (b) Particle initialization at the end of the BIPP algorithm.

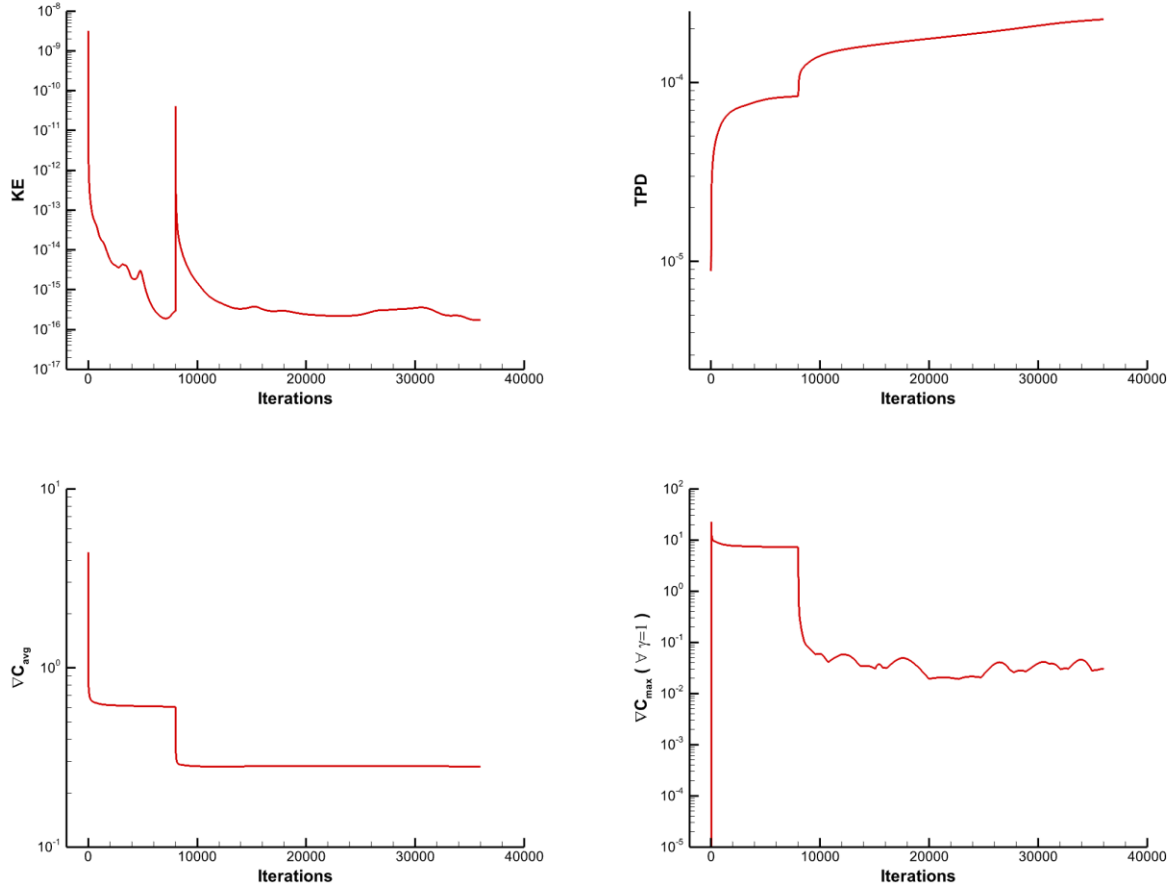


Figure 10 Evolution of (a) KE, (b) TPD, (c) $|\nabla C|_{avg}$, and (d) $|\nabla C|_{max}$ for particles with $\gamma=1$, during the BIPI algorithm for the 2D bunny case.

5 Conclusion

The Boundary Integral based Particle Initialization (BIPI) algorithm proposed here represents a significant advancement in particle initialization techniques for Smooth Particle Hydrodynamics (SPH) simulations in the following ways:

Firstly, BIPI revolutionizes particle initialization by eliminating the need for virtual particle layers, directly utilizing boundary information through boundary integrals. This approach streamlines the modeling process for complex boundaries, enhancing efficiency and accuracy.

Secondly, unlike traditional initialization models that directly solve the momentum equation, BIPI simplifies the process to a particle shifting algorithm. This algorithm is applied to both interior

particles and those near the boundary, with the latter utilizing boundary integral formulation to accommodate truncated kernels.

Moreover, BIPI ensures a uniform particle configuration by minimizing concentration gradient errors. This optimization enhances simulation accuracy and stability, which is crucial for achieving reliable results.

Additionally, by implementing a boundary force, BIPI addresses the challenge of artificial compression of particle volume near the boundary. This prevents undesirable distortions, maintains the particle distribution's integrity, and allows faster convergence to conditionally stable particle configuration.

Lastly, BIPI optimizes computational efficiency by prioritizing particle fitting along the boundary before redistributing particles throughout the domain. This strategic approach minimizes computational overhead and streamlines the initialization process.

References

- [1] Monaghan JJ. Smoothed Particle Hydrodynamics. *Annu Rev Astron Astrophys* 1992;30:543–74. <https://doi.org/10.1146/annurev.aa.30.090192.002551>.
- [2] Liu MB, Liu GR. Smoothed Particle Hydrodynamics (SPH): an Overview and Recent Developments. *Archives of Computational Methods in Engineering* 2010;17:25–76. <https://doi.org/10.1007/s11831-010-9040-7>.
- [3] Price DJ. Smoothed particle hydrodynamics and magnetohydrodynamics. *J Comput Phys* 2012. <https://doi.org/10.1016/j.jcp.2010.12.011>.
- [4] Oger G, Doring M, Alessandrini B, Ferrant P. An improved SPH method: Towards higher order convergence. *J Comput Phys* 2007;225:1472–92. <https://doi.org/10.1016/J.JCP.2007.01.039>.
- [5] Colagrossi A, Antuono M, Le Touzé D. Theoretical considerations on the free-surface role in the smoothed-particle-hydrodynamics model. *Phys Rev E Stat Nonlin Soft Matter Phys* 2009;79:056701. <https://doi.org/10.1103/PHYSREVE.79.056701/FIGURES/11/MEDIUM>.

- [6] Colagrossi A, Bouscasse B, Antuono M, Marrone S. Particle packing algorithm for SPH schemes. *Comput Phys Commun* 2012;183:1641–53. <https://doi.org/10.1016/J.CPC.2012.02.032>.
- [7] Negi P, Ramachandran P. Algorithms for uniform particle initialization in domains with complex boundaries. *Comput Phys Commun* 2021;265:108008. <https://doi.org/10.1016/J.CPC.2021.108008>.
- [8] Desjardin PE, Bojko BT, Mcgurn MT. Initialization of high-order accuracy immersed interface CFD solvers using complex CAD geometry. *INTERNATIONAL JOURNAL FOR NUMERICAL METHODS IN ENGINEERING Int J Numer Meth Engng* 2017;109:487–513. <https://doi.org/10.1002/nme.5294>.
- [9] Xu R, Stansby P, Laurence D. Accuracy and stability in incompressible SPH (ISPH) based on the projection method and a new approach. *J Comput Phys* 2009;228:6703–25. <https://doi.org/10.1016/J.JCP.2009.05.032>.
- [10] Lind SJ, Xu R, Stansby PK, Rogers BD. Incompressible smoothed particle hydrodynamics for free-surface flows: A generalised diffusion-based algorithm for stability and validations for impulsive flows and propagating waves. *J Comput Phys* 2012;231:1499–523. <https://doi.org/10.1016/J.JCP.2011.10.027>.
- [11] Michel J, Vergnaud A, Oger G, Hermange C, Le Touzé D. On Particle Shifting Techniques (PSTs): Analysis of existing laws and proposition of a convergent and multi-invariant law. *J Comput Phys* 2022;459:110999. <https://doi.org/10.1016/j.jcp.2022.110999>.
- [12] Oger G, Marrone S, Le Touzé D, de Leffe M. SPH accuracy improvement through the combination of a quasi-Lagrangian shifting transport velocity and consistent ALE formalisms. *J Comput Phys* 2016. <https://doi.org/10.1016/j.jcp.2016.02.039>.
- [13] Lee E-S, Moulinec C, Xu R, Violeau D, Laurence D, Stansby P. Comparisons of weakly compressible and truly incompressible algorithms for the SPH mesh free particle method. *J Comput Phys* 2008;227:8417–36. <https://doi.org/10.1016/J.JCP.2008.06.005>.
- [14] Morris JP, Fox PJ, Zhu Y. Modeling Low Reynolds Number Incompressible Flows Using SPH. *J Comput Phys* 1997;136:214–26. <https://doi.org/10.1006/JCPH.1997.5776>.

- [15] Kulasegaram S, Bonet J, Lewis RW, Profit M. A variational formulation based contact algorithm for rigid boundaries in two-dimensional SPH applications. *Comput Mech* 2004;33:316–25. <https://doi.org/10.1007/s00466-003-0534-0>.
- [16] Mayrhofer A, Rogers BD, Violeau D, Ferrand M. Investigation of wall bounded flows using SPH and the unified semi-analytical wall boundary conditions. *Comput Phys Commun* 2013;184:2515–27. <https://doi.org/10.1016/J.CPC.2013.07.004>.
- [17] Mayrhofer A, Ferrand M, Kassiotis C, Violeau D, Morel F-X, Ferrand M, et al. Unified semi-analytical wall boundary conditions in SPH: analytical extension to 3-D 2015;68:15–34. <https://doi.org/10.1007/s11075-014-9835-y>.
- [18] Chiron L, de Leffe M, Oger G, Le Touzé D. Fast and accurate SPH modelling of 3D complex wall boundaries in viscous and non viscous flows. *Comput Phys Commun* 2019;234:93–111. <https://doi.org/10.1016/J.CPC.2018.08.001>.
- [19] Monaghan JJ. Simulating Free Surface Flows with SPH. *J Comput Phys* 1994;110:399–406. <https://doi.org/10.1006/JCPH.1994.1034>.
- [20] Litvinov S, Hu XY, Adams NA. Towards consistence and convergence of conservative SPH approximations. *J Comput Phys* 2015;301:394–401. <https://doi.org/10.1016/J.JCP.2015.08.041>.
- [21] Jiang M, Zhou Y, Wang R, Southern R, Jun Zhang J, Diff D. Blue Noise Sampling using an SPH-based Method. *ACM Trans Graph* 2015;34. <https://doi.org/10.1145/2816795.2818102>.
- [22] Fu L, Ji Z. An optimal particle setup method with Centroidal Voronoi Particle dynamics. *Comput Phys Commun* 2019;234:72–92. <https://doi.org/10.1016/J.CPC.2018.08.002>.
- [23] Zhu Y, Zhang C, Yu Y, Hu X. A CAD-compatible body-fitted particle generator for arbitrarily complex geometry and its application to wave-structure interaction. *Journal of Hydrodynamics* 2021;33:195–206. <https://doi.org/10.1007/S42241-021-0031-Y/METRICS>.

- [24] Yu Y, Zhu Y, Zhang C, Haidn OJ, Hu X. Level-set based pre-processing techniques for particle methods ☆. *Comput Phys Commun* 2023;289:108744. <https://doi.org/10.1016/j.cpc.2023.108744>.
- [25] Boregowda P, Liu GR. On the accuracy of SPH formulations with boundary integral terms. *Math Comput Simul* 2023;210:320–45. <https://doi.org/10.1016/J.MATCOM.2023.03.018>.
- [26] Domínguez JM, Crespo AJC, Barreiro A, Domínguez JM, Crespo AJC, Barreiro A, et al. Development of a new pre-processing tool for SPH models with complex geometries, Hamburg, Germany: 6th international SPHERIC workshop; 2011.
- [27] Zhang C, Rezavand M, Zhu Y, Yu Y, Wu D, Zhang W, et al. SPHinXsys: An open-source multi-physics and multi-resolution library based on smoothed particle hydrodynamics. *Comput Phys Commun* 2021;267:108066. <https://doi.org/10.1016/J.CPC.2021.108066>.
- [28] Leroy A, Violeau D, Ferrand M, Kassiotis C. Unified semi-analytical wall boundary conditions applied to 2-D incompressible SPH. *J Comput Phys* 2014;261:106–29. <https://doi.org/10.1016/j.jcp.2013.12.035>.
- [29] Liu GR, Liu MB. *Smoothed Particle Hydrodynamics*. WORLD SCIENTIFIC; 2003. <https://doi.org/10.1142/5340>.